Proposal for simultaneous analysis of fluorescence intensity Fluctuations and Resonance Energy Transfer (iFRET) measurements

Michael R. Stoneman[1], Gabriel Biener[1] and Valerică Raicu[1,2,*]

[1]*Physics Department, University of Wisconsin-Milwaukee, Milwaukee, Wisconsin, USA*
[2]*Department of Biological Sciences, University of Wisconsin-Milwaukee, Milwaukee, Wisconsin, USA.*

Abstract

Resonance energy transfer (RET) and fluorescence fluctuation spectroscopies (FFS) are powerful fluorescence-based techniques for quantifying the self-association of membrane receptors within oligomeric complexes in living cells. However, RET spectrometry's ability to extract information on the detailed quaternary structure of oligomers sometimes rests on assumptions regarding the relative abundances of oligomers of different sizes, while FFS techniques may provide oligomer size information but not quaternary structure details, as they lack a probe for inter-molecular distances. In this report, we introduce a method which we termed "intensity fluctuations and resonance energy transfer" (iFRET), which combines analysis of donor and acceptor intensity fluctuations with RET efficiency determination. Because the three measured quantities each have a unique dependence on the acceptor mole fraction (X_A), simultaneous global fitting of all three dramatically reduces ambiguity in the data fitting and choice of the most appropriate fitting model. We demonstrate the effectiveness of the method on simulated brightness and RET efficiency data incorporating mixtures of monomers, dimers, and tetramers and show that iFRET analysis provides a major improvement in both identifying the correct quaternary structure model and extracting the relative abundances of the monomers, dimers, and tetramers. Conceivably, the enhanced resolution of iFRET could potentially provide insight into the functional significance of receptor oligomerization in the presence and absence of cognate ligands.

*Correspondence should be addressed to V. Raicu at vraicu@uwm.edu

1. Introduction

Interactions between membrane receptors are known to play a vital role in a large number of biological processes [1, 2]. However, understanding the functional roles of receptor interactions has proved challenging, in part because of the difficulty in characterizing the quaternary organization of proteins in their native environment [3]. Many protein assemblies are known to engage in dynamic association/disassociation equilibria, thus creating a concentration dependent mixture of different sized oligomers, further expanding the concept of quaternary structure and thereby complicating the analysis. Several *in vitro* and *in vivo* techniques have been developed in an attempt to augment knowledge of the various aspects of protein–protein interactions. Of these techniques, two classes of methods have been established which are at the forefront of measuring interactions *in vivo*: Resonance Energy Transfer [4-9] (RET) and Fluorescence Fluctuation Spectroscopy [10-13] (FFS).

RET is a physical process in which weak electronic coupling occurring between an electronically excited molecule (donor) and an adjacent molecule in its ground state (acceptor) results in a non-radiative transfer of energy [14, 15]. The radiationless transfer of energy is strongly dependent on distance and occurs when the two molecules are <10 nm from one another, coinciding nicely with the expected distances between monomer units in protein complexes. By measuring and analyzing the apparent efficiency of energy transfer (E_{app}) from a population of donor and acceptor molecules, some of which may be interacting, rich information regarding the relative distance and orientation of the molecules with respect to one another can be extracted. A multitude of studies have shown the effectiveness of utilizing RET for obtaining quantitative information on protein-protein interactions [16-22], including detailed information about the size and structure of membrane receptor complexes [23-27].

Typical RET-based approaches for quantifying protein-protein interactions rely on plotting the average E_{app} against the ratio of the donor to acceptor concentrations in the sample [28], the fraction of donors or acceptors [29-31], or the total concentration of donors and acceptors [28, 32, 33], and then fitting a model derived from the kinetic theory of RET [34] to the experimental data using the concentration of oligomers as a fitting parameter. Unfortunately, this method only works well if the number of protomers within an oligomeric complex and the geometry of the oligomer are a priory known (and fixed during the fitting process) [34], since otherwise an unlimited number of combinations between geometrical parameters and pairwise RET efficiencies fit the data equally well. To adddress this difficulty, we have previously introduced FRET spectrometry [24-26, 35], a method which interprets distributions of pixel-level E_{app} values, as opposed to averages over large regions [36], using oligomeric models with various quaternary structures. For every quaternary structure, several possible ways exist of arranging the donor and acceptor (i.e., choosing their locations) within an oligomeric complex, and each arrangement, or oligomer configuration, corresponds to a specific peak in the E_{app} distribution. The collection of various peak positions, termed a RET *spectrum* (or *spectrogram*), represents a unique fingerprint corresponding to a particular oligomeric structure [35, 37]. From the quaternary structure model which best fits the measured E_{app} distributions, detailed geometrical parameters and pairwise RET efficiency values can then be extracted and combined with the average-based approaches to obtain the relative abundance of various oligomer species comprising the sample [29]. The main advantage of the

RET spectrometry approach is that it is currently the only *in vivo* method that allows determination of interprotomeric distances (i.e., quaternary structure) and proportions of different structures. Its main challenge is that it necessitates the use of rather complicated analysis procedures, which are difficult to implement outside of optics labs and may be time consuming too.

Fluorescence fluctuation spectroscopy encompasses a multitude of techniques that measure the diffusion coefficients, concentration, and molecular brightness of fluorescently labeled biomolecules by analyzing the correlations and/or distributions of fluorescence intensities [11, 38-41]. The subset of FFS techniques which analyze the moments of fluorescence intensity distributions provide information on the average oligomeric size for the fluorescently labeled molecules within a complex by introducing the molecular brightness, i.e., the width of the distribution of intensities for fluorescent molecules over a given time period [42-46]. If two identical proteins, each tagged with the same fluorescent label, form a complex, then this dimeric complex will have twice the number of fluorophores than the single monomers diffusing alone, and hence twice the molecular brightness. When this oligomer enters the excitation volume of a focused laser beam, it will cause a broader distribution of fluorescence intensities than single monomers. Because the molecular brightness of a complex of fluorescently labeled proteins scales linearly with the size of the complex, the moment-based FFS techniques are effective for determining the average size a protein complex forms (e.g., monomer, dimer, higher order oligomer) [47-50]. The main advantage of these methods is simplicity in operation and speed, while their main limitation is that they do not provide information on individual oligomer sizes or geometry but rather an average over mixtures of monomers, dimers, oligomers, etc. A recently developed moment-based approach, named two-dimensional fluorescence intensity fluctuation (2D FIF) spectrometry [51, 52], provides quantitative information on the relative abundance of various sized protein oligomers as a function of receptor concentration. This method is both fast and capable of extracting oligomer size, but does not provide information on oligomer geometry.

The advent of laser scanning microscopes which incorporate spectral resolution [53-58] has greatly enhanced the potential of using fluorescence based techniques for quantifying protein interactions. The acquisition of an entire fluorescence spectrum enables overlapping spectral profiles to be separated according to the distinct shapes of the spectra, using spectral unmixing [23, 28, 59-61], which avoids the artifact of spectral crosstalk between fluorescent tags [62]. Spectrally resolved imaging is ideal for RET measurements because it allows for the quantitation of both donor and acceptor fluorescence intensity levels, from which the RET efficiency can be straightforwardly calculated. Likewise, a number of molecular brightness based FFS methods have incorporated multi-color measurements to enhance their effectiveness in separating mixtures of multiple species. Extensions to both Number and Brightness as well as Photon Counting Histogram techniques, termed ccN&B [63] and dual color PCH [64], respectively, measure the cross correlation of fluorescence amplitude fluctuations from two different colors, obtained from repeated measurements over time at a fixed position in a sample. More recently, Faust et al. have extended molecular brightness based methods which measure fluctuations in the spatial domain with multi-color analysis in a technique called Two-Color Spatial Cumulant Analysis (2c-SpCA) [65]. Unfortunately, to date none of these multi-color approaches have incorporated a measurement of RET efficiency into their analysis procedure, and are therefore constrained to either resolving mixtures of non-interacting species to qualitatively probe the presence of

heteromeric interactions in the presence of RET, or quantifying the hetero-oligomerization of protein complexes when no RET is occurring between the fluorescent probes. Therefore, detailed structural information regarding protein oligomers can not be extracted from any of these approaches.

In this work, we propose a rather simple and robust multi-parameter approach which combines the analysis of donor and acceptor intensity fluctuations (IF) with RET efficiency values in a global analysis procedure called iFRET. IF or RET measurements on their own can struggle to discriminate between fitting models incorporating mixtures of monomers, dimers, and higher order oligomers, when there is no a priori knowledge of either the sample composition or structure formed by interactions, as is often the case for measurements within living cells or other complex systems. We show that simultaneous measurement and global analysis of molecular brightness and RET data greatly enhances the resolution of information extracted when compared to the capabilities of the individual techniques alone. Because the two sets of measurements provide complementary information to one another, both structural information regarding the distances between protomers in a protein complex and the composition of the sample, i.e., percentage of monomers, dimers and higher order oligomers, were obtainable when the two techniques were combined. The increased resolution of iFRET arises from two key aspects of the method, which help restrict the variability and ambiguity in data fitting routines. The first aspect requires the measurement of relative concentrations of the donor and acceptor molecules. RET will alter the apparent brightness values of both the donor and acceptor populations, with the amount of change dependent not only on the value of RET efficiency but also on the acceptor mole fraction (X_A), i.e., the fraction of total fluorophores which are acceptors. The nonlinear dependence of fluorescence intensity fluctuations and RET efficiency on X_A is beneficial in that it serves as an additional measured parameter to the multi-modal approach. The second aspect is that all three data sets are simultaneously (or globally) fit with a common set of parameters. The simultaneous fitting greatly constrains the fitting parameter space and thereby helps restrict the choice of model which accurately predicts the data, increasing the accuracy with which the underlying system can be described.

We implemented iFRET on computer simulated brightness and RET efficiency data for mixtures of monomers, dimers, and higher order oligomers in the presence of experimental camera noise. Our results demonstrated the ability to extract two otherwise difficult pieces of information: (1) the relative abundances (or species fractions) and (2) geometrical parameters of each of each oligomeric complex comprising the mixture, even when there was no single dominant species in the mixture.

2. Methods

The main goal of this work is to demonstrate the value of simultaneously quantifying fluorescence fluctuation data from both donor and acceptors along with the RET occurring between the two. To that end, we must first develop a formalism for modeling fluorescence intensity fluctuations of donors forming oligomeric complexes with acceptors, and vice versa. The fluorescence signal at the complex level is the key component in modeling intensity fluctuations of donor and acceptor molecules individually. Because the fluorescence intensity of donors and acceptors in oligomeric

complexes depend on the RET occurring between protomers in the complex, we will first summarize the previously published kinetic theory of RET in multimeric complexes [34]. We will then describe the average donor and acceptor fluorescence emitted from individual oligomer complexes using the same theory. Finally, a formula for modeling the intensity fluctuations will be given.

2.1. Theoretical model for the RET efficiency of an oligomeric complex

Before we proceed, let us define a few quantities and variables of interest. The size of the oligomer (denoted by an integer, n) represents the total number of molecules (i.e., donors plus acceptors), or protomers, within an oligomer consisting of k donors and $n - k$ acceptors. For each pair of k and n-k values, there are $\binom{n}{k} = \frac{n!}{k!(n-k)!}$ possible ways of placing the donors and acceptors within the oligomer (see figure 1). Each of these ways are examples of different configurations, and are indexed by the letter q.

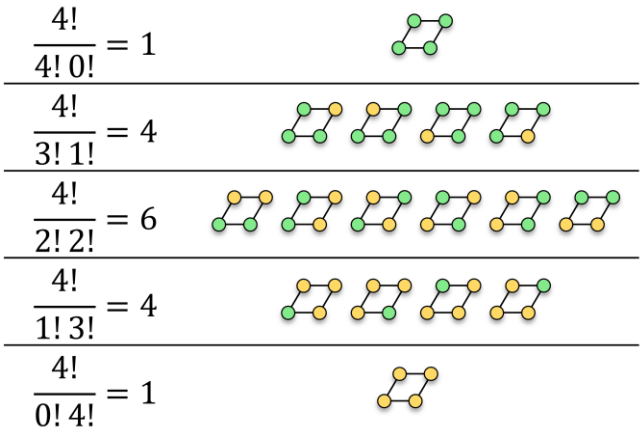

Figure 1. All possible configurations, for each value of k, assumed by donors (green circles) and acceptors (yellow circles) in an oligomer of size $n = 4$.

For a donor (D) in the close proximity of one or more acceptors (A), for example in an oligomer complex of size n>2, there can be a number of independent de-excitation pathways related to energy transfer equal to the number of acceptors in a complex; these are in addition to the usual non-radiative and radiative (i.e., fluorescence-producing) de-excitation pathways. Therefore the efficiency of energy transfer occurring between a donor, i, and a single acceptor, j, can be found by dividing the rate of energy transfer between the donor and acceptor, $\Gamma_{i,j}^{RET}$, by the sum of rates for all de-excitation pathways of the donor, as follows [34]:

$$E_{i,j,n,k,q} = \frac{\Gamma_{i,j}^{RET}}{\Gamma^{r,D} + \Gamma^{nr,D} + \sum_{j=1}^{n-k} \Gamma_{i,j}^{RET}} \quad (1)$$

Here $\Gamma^{r,D}$ and $\Gamma^{nr,D}$ are the radiative and non-radiative decay rates of the donor, respectively. The sum over j in equation (1) represents all acceptors in close proximity to the donor, i.e., acceptors within the same complex. The total RET efficiency occurring for a single donor, i, in a complex of size n, number of donors k, and configuration q, is simply the sum of the individual RET efficiencies occurring between the donor and each acceptor in the complex:

$$E_{i,n,k,q} = \sum_{j=1}^{n-k} E_{i,j,n,k,q} = \frac{\sum_{j=1}^{n-k} \Gamma_{i,j}^{RET}}{\Gamma^{r,D} + \Gamma^{nr,D} + \sum_{j=1}^{n-k} \Gamma_{i,j}^{RET}} \quad (2)$$

The set of distances between a donor and each of the acceptors in a particular configuration will be different for each individual donor in said configuration. Therefore, the individual donors within an oligomeric complex can have completely different sets of de-excitation pathways, and thereby exhibit entirely different RET efficiencies. The average RET efficiency per donor in the complex can be found by averaging the RET values of each individual donor:

$$E_{n,k,q} = \frac{1}{k} \sum_{i=1}^{k} E_{i,n,k,q} \quad (3)$$

An example of the computed $E_{n,k,q}$ values for each possible configuration of a specific tetrameric oligomer are listed in Supplementary Figure 1, along with the average donor and acceptor signal (formulas derived below).

2.2. Fluorescence intensity of donors and acceptors in oligomeric complexes

The fluorescence emitted by each donor molecule within an oligomeric complex of size *n* not only depends on the fluorescent properties of the donor itself, but also its location relative to acceptor molecules within the complex. The brightness of a donor molecule, *i*, within an oligomer of size *n*, containing *k* donors, and in configuration *q*, can be broken into three factors, as follows:

$$\mathcal{E}_{i,n,k,q}^{DA}(\lambda_{ex}) = \xi \Gamma^{ex,D} Q_{i,n,k,q}^{DA} \quad (4)$$

where $\Gamma^{ex,D}$ represents how efficiently the donor molecules are excited at the center of a focused laser beam of wavelength λ_{ex}, i.e., the excitation rate constant, and ξ is a constant incorporating measuring system parameters, namely the collection efficiency of the photons, gain of the measuring system, and measurement integration time. Finally, Q^{DA} represents the quantum yield of the donor molecule in the presence of nearby acceptors. Because the nearby acceptors present additional de-excitation pathways for the donor to lose energy non-radiatively, Q^{DA} is lower than the quantum yield of the donor when no acceptors are present, which is represented by Q^{D}. Each donor molecule will display a quantum yield dependent on the number and placement of acceptor molecules within the complex. The quantum yield of a donor in the presence of acceptors (i.e., RET) can be related to Q^{D} and the RET efficiency via the relation [34]:

$$Q_{i,n,k,q}^{DA} = Q^{D}\left(1 - E_{i,n,k,q}\right) \quad (5)$$

where $E_{i,n,k,q}$ is the RET efficiency of the i^{th} donor, given by equation (2). By combining equations (4) and (5), the amount of fluorescence signal detected from a donor molecule can be written as:

$$\mathcal{E}_{i,n,k,q}^{DA}(\lambda_{ex}) = \varepsilon_{m}^{D}\left(1 - E_{i,n,k,q}\right) \quad (6)$$

where $\varepsilon_{m}^{D}(\lambda_{ex}) = \xi \Gamma^{ex,D} Q^{D}$ represents the molecular brightness of the donor, i.e., the average detected signal of a monomeric form of the donor for a given exposure time. Finally, the total fluorescence measured for a particular oligomer configuration can be written as a sum of $\mathcal{E}_{i,n,k,q}^{DA}$ over the total number of donors, k, in the complex:

$$\mathcal{E}_{n,k,q}^{DA}(\lambda_{ex}) = \sum_{i=1}^{k} \mathcal{E}_{i,n,k,q}^{DA} = \varepsilon_{m}^{D} k\left(1 - E_{n,k,q}\right) \quad (7)$$

Here $E_{n,k,q}$ is the average RET efficiency per donor of the complex indexed by k and q, as given by equation (3).

Similarly, the total fluorescence detected from an acceptor molecule, *j*, within an oligomer complex depends not only on the fluorescent properties of the acceptor itself, but also its location relative to donor molecules within the complex:

$$\mathcal{E}^{AD}_{j,n,k,q}(\lambda_{ex}) = \xi\, \Gamma^{ex,AD}_{j,n,k,q} Q^A \tag{8}$$

Unlike the donor case, the quantum yield, Q^A, of the acceptor molecules remains unchanged in the presence of donors, however the excitation rate constant of the acceptor, $\Gamma^{ex,AD}_{j,n,k,q}$, increases due to additional excitations coming from nearby donor molecules:

$$\Gamma^{ex,AD}_{j,n,k,q} = \Gamma^{ex,A} + \Gamma^{ex,D} \sum_{i=1}^{k} E_{i,j,n,k,q} \tag{9}$$

where the first term in equation (9) represents the rate of direct excitation of the acceptor molecule by the laser, and the second term is the rate of excitation via energy transfer from donor molecules. Combining equations (8) and (9), the total signal detected from a single acceptor molecule in a complex with donors can then be written as:

$$\mathcal{E}^{AD}_{j,n,k,q}(\lambda_{ex}) = \varepsilon^A_m + \varepsilon^D_m \frac{Q^A}{Q^D} \sum_{i=1}^{k} E_{i,j,n,k,q} \tag{10}$$

where the molecular brightness of a monomeric acceptor, $\varepsilon^A_m(\lambda_{ex}) = \xi \Gamma^{ex,A} Q^A$, has been introduced. The total amount of acceptor signal detected for the entire complex is found by summing over the contributions from each acceptor in said complex:

$$\mathcal{E}^{AD}_{n,k,q} = (n-k)\varepsilon^A_m + \varepsilon^D_m \frac{Q^A}{Q^D} \sum_{i=1}^{k} \sum_{j=1}^{n-k} E_{i,j,n,k,q} \tag{11}$$

The summation on the right side of equation (11) is simply the number of donors in the complex times the average RET efficiency per donor, as given by equation (3). Therefore, equation (11) simplifies to:

$$\mathcal{E}^{AD}_{n,k,q} = (n-k)\varepsilon^A_m + \varepsilon^D_m \frac{Q^A}{Q^D} k E_{n,k,q} \tag{12}$$

2.3. Calculation of RET efficiency from integrated fluorescence spectra

When complete emission spectra of the donors and acceptors fluorescence are available in RET experiments [23, 28], expressions for the integrated emission spectra of donors in the presence of acceptors (F^{DA}) and acceptors in the presence of donors (F^{AD}) may be written for mixtures of various sized oligomers as [34]:

$$F^{DA}(\lambda_{ex}) = \sum_n \mu_n \sum_{k=1}^{n} (1-X_A)^k (X_A)^{(n-k)} \sum_{q=1}^{\binom{n}{k}} \mathcal{E}^{DA}_{n,k,q} \tag{13}$$

$$F^{AD}(\lambda_{ex}) = \sum_n \mu_n \sum_{k=0}^{n-1} (1-X_A)^k (X_A)^{(n-k)} \sum_{q=1}^{\binom{n}{k}} \mathcal{E}^{AD}_{n,k,q} \tag{14}$$

where μ_n represents the total concentration of an oligomer of size *n*, and X_A the total fraction of molecules which are acceptors (whether associated within oligomers or remaining as free monomers). The summation over *n* in equations (13) and (14) represents the total signal emanating from complexes of all sizes in the mixture. The contribution to the signal from monomers in equations (13) and (14), i.e., when *n* = 1, arises from only a single term in the sum; in this case $\mathcal{E}^{DA}_{1,1,1}$ is equal to the monomeric brightness of the donor, ε^D_m, which has been introduced in the preceeding section. Similarily, $\mathcal{E}^{AD}_{1,1,1}$ is equal to the monomeric brightness of the acceptor, ε^A_m, for the chosen excitation wavelength.

The apparent RET efficiency, defined as the ratio between the donor fluorescence lost due to RET and the fluorescence of the donor in the absence of acceptor, can be determined from the integrated fluorescence spectra of the donor and acceptor using the following relation [34]:

$$E_{app} = 1 - \frac{F^{DA}(\lambda_{ex})}{F^{D}(\lambda_{ex})} \tag{15}$$

where $F^{D}(\lambda_{ex})$ is the wavelength-integrated fluorescence expected from the donor if no acceptor was present. In order to determine the value of $F^{D}(\lambda_{ex})$, we break up the total fluorescence from donors and acceptors into two quantities [23, 34]:

$$F^{DA}(\lambda_{ex}) = F^{D}(\lambda_{ex}) - F_{D}^{FRET} \tag{16}$$

$$F^{AD}(\lambda_{ex}) = F^{A}(\lambda_{ex}) + \frac{Q^{A}}{Q^{D}} F_{D}^{FRET} \tag{17}$$

where F_{D}^{FRET} is the loss of emission from the donor due to RET. The total fluorescence expected from the acceptor if no donor was present, $F^{A}(\lambda_{ex})$, can be set to zero if a donor-acceptor pair is chosen such that there exists an excitation wavelength in which the acceptor is not directly excited. In this scenario, equations (15)-(17) can be combined to write an expression for E_{app} as a function of donor and acceptor integrated intensity values [23]:

$$E_{app} = \frac{F^{AD}}{\frac{Q_A}{Q_D} \cdot F^{DA} + F^{AD}} \tag{18}$$

In other situations, where both the donors and acceptors are excited – either by necessity or by choice – alternative ways exist of computing the RET efficiency as well as the donor and acceptor concentrations across all oligomeric species [33].Equation (18) has previously been used to compute the experimentally measured RET efficiency for every pixel in an image [23]. An average RET efficiency, E_{ave}, also may be computed over a larger segment containing multiple pixels by first computing the average values of measured or simulated F^{DA} and F^{AD} over all the pixels in the segment, and inserting those values into equation (18). Herein, computer simulated values of E_{ave} are then modeled theoretically and interpreted using equation (S2) of Supplementary Note 1.

2.4. Modeling fluctuations in donor and acceptor fluorescence intensities

The core idea behind fluctuation spectroscopy is quantifying fluctuations in fluorescence intensity values, obtained either by repeated measurement of a pixel in time, or by recording intensities from multiple adjacent pixels. The amplitude of these intensity fluctuations carries information related to the molecular brightness of the molecule, which in turn, scales linearly with the size of the molecule. The apparent molecular brightness, ε, of the molecules comprising the sample can be extracted from a straightforward set of intensity measurements by measuring the variance, σ^2, and mean, $\langle I \rangle$, of said intensity distribution, using the following relation [51, 66]:

$$\varepsilon_{eff} = \frac{\sigma^2 - \sigma_{DET}^2}{\langle I \rangle \gamma} \tag{19}$$

where γ is a shape factor which depends on the shape of the laser PSF as well as the geometry of the sample, and σ_{DET}^2 the variance due to shot noise of the signal and noise characteristics of the detector. When a photon counting detector is used, σ_{DET}^2 is simply equal to $\langle I \rangle$. If the sample under investigation is comprised of multiple types of oligomer species, e.g., monomers, dimers, trimers, etc. then the measured brightness given by equation (19) reflects a nonlinear combination of the

molecular brightness, ε_l, of each species in the sample, weighted by the relative proportion, μ_l, of each respective species [50]:

$$\varepsilon_{eff,theo} = \frac{\sum_l \varepsilon_l^2 \mu_l}{\sum_l \varepsilon_l \mu_l} \tag{20}$$

When the molecules in the sample are tagged with two different fluorescent labels, then we can actually recover two different distributions of intensities, i.e., one from the donor molecules and one from the acceptor molecules. Therefore, based on equation (20) we can write down an expression for the apparent molecular brightness of the donor,

$$\varepsilon_{eff}^{DA} = \frac{\sigma_{I_D}^2 - \sigma_{DET}^2}{\langle I_D \rangle \gamma} \tag{21}$$

where $\sigma_{I_D}^2$ and $\langle I_D \rangle$ represent the variance and mean of the intensity distribution for the donor, and another expression for the apparent molecular brightness of the acceptor,

$$\varepsilon_{eff}^{AD} = \frac{\sigma_{I_A}^2 - \sigma_{DET}^2}{\langle I_A \rangle \gamma} \tag{22}$$

where $\sigma_{I_A}^2$ and $\langle I_A \rangle$ represent the variance and mean of the measured acceptor intensities.

When RET is occurring between the two fluorescent tags, the interpretation of equations (21) and (22) requires additional considerations:

(i) The pathways of energy transfer from donors to nearby acceptors reduces the intensity of the donor and increases that of the acceptor, which thereby alters the value of ε_{eff}^{DA} and ε_{eff}^{AD}.

(ii) From the standpoint of molecular brightness, the different possible donor and acceptor configurations within each oligomer of a certain size *n* result in completely different molecular species. In other words, different brightness values correspond to different *k* values, and even different configurations, *q,* within a particular *k* value. A simple example illustrating these points can be drawn from a solution of pure dimers. Three different configurations of dimer molecules will be present in the sample: DD, DA, and AA dimers. When analyzing the intensity fluctuations from donor-only signals, DD dimers will have a molecular brightness twice that of the monomeric form of the donor fluorophore, AA dimers will have a brightness of zero, and the DA dimer will have a reduced brightness, when compared to a monomeric donor fluorophore, due to RET occurring between D and A. Therefore, the measured brightness value will be a nonlinear combination of the brightness values from all configurations, even for a solution with only a single oligomer size. Because of this inherent complexity in even the simplest of systems, one of the questions proposed in this manuscript is whether calculation of ε_{eff}^{DA} and ε_{eff}^{AD} delivers any meaningful insight to the molecules being studied.

Since the apparent molecular brightness of mixtures of donors forming complexes with acceptors is a nonlinear combination of the brightness values from all oligomer configurations, we can use equation (20) for the apparent molecular brightness of a mixture of multiple species, and simply treat each of the 2^n possible oligomer configurations as an independent molecular species within the mixture. The molecular brightness of each individual species is the average fluorescence signal of the complex, which we have presented in the preceding section. By combining equations (7) and (12), we obtain a formula for the apparent brightness of donors:

$$\varepsilon_{eff,n}^{DA} = \frac{\sum_{k=1}^{n} \mu_{n,k} \sum_{q=1}^{\binom{n}{k}} \left(\varepsilon_{n,k,q}^{DA}\right)^2}{\sum_{k=1}^{n} \mu_{n,k} \sum_{q=1}^{\binom{n}{k}} \varepsilon_{n,k,q}^{DA}} = \frac{\varepsilon_m^D \sum_{k=1}^{n} \mu_{n,k} \sum_{q=1}^{\binom{n}{k}} \left(1-E_{n,k,q}\right)^2 k^2}{\sum_{k=1}^{n} \mu_{n,k} \sum_{q=1}^{\binom{n}{k}} \left(1-E_{n,k,q}\right) k} \tag{23}$$

At first glance, equation (23) does not ease any concerns regarding the complexity of interpreting ε_{eff}^{DA}, as there are 2^n terms in both the numerator and denominator, with each term involving a weighting factor, $\mu_{n,k}$, which represents the concentration of that particular oligomer configuration. However, all values of $\mu_{n,k}$ are determined from only two parameters, the total oligomer concentration and X_A, as given by the following equation:

$$\mu_{n,k} = \mu_n (1 - X_A)^k (X_A)^{(n-k)} \tag{24}$$

The term μ_n does cancel out in equation (23), for the scenario when only a single oligomer size is being taken into consideration. However, it does become an important factor when mixtures of various sized oligomers are considered. Taking equation (24) into account, the set of free parameters to be inserted into equation (23) is limited to the following: ε_m^D, X_A, and the RET efficiency of each oligomeric complex. ε_m^D, is a measurable quantity typically found by calibration measurements on a monomeric form of the donor construct. The value of X_A can be determined from measurements of the sample at two excitation wavelengths [29]. Therefore, the only adjustable parameter left is the $E_{n,k,q}$, which is completely defined by the oligomer structural model being tested.

A similar formula may be written for the apparent brightness obtained from monitoring fluctuations in the acceptor signal:

$$\varepsilon_{eff,n}^{AD} = \frac{\sum_{k=0}^{n-1} \mu_{n,k} \sum_{q=1}^{\binom{n}{k}} \left(\varepsilon_{n,k,q}^{AD}\right)^2}{\sum_{k=0}^{n-1} \mu_{n,k} \sum_{q=1}^{\binom{n}{k}} \varepsilon_{n,k,q}^{AD}} = \frac{\sum_{k=0}^{n-1} \mu_{n,k} \sum_{q=1}^{\binom{n}{k}} \left[(n-k)\varepsilon_m^A + \varepsilon_m^D \frac{Q^A}{Q^D} k E_{n,k,q}\right]^2}{\sum_{k=0}^{n-1} \mu_{n,k} \sum_{q=1}^{\binom{n}{k}} \left[(n-k)\varepsilon_m^A + \varepsilon_m^D \frac{Q^A}{Q^D} k E_{n,k,q}\right]} \tag{25}$$

In addition to the parameters discussed above, equation (25) necessitates a value for ε_m^A, the molecular brightness of a monomeric form of the acceptor molecule, which is also obtainable from calibration measurements. Choosing a donor-acceptor pair and excitation wavelength such that the acceptor molecule is not directly excited by the laser removes the need for a calibration measurement to determine ε_m^A.

Equations (23) and (25) (taken together with equation (24)) may be extended rather easily to incorporate monomers as well as additional oligomer sizes by summing over all terms in each of their respective oligomer species in both the numerator and denominator:

$$\varepsilon_{eff,theo}^{X}(X_A) = \frac{\sum_n \mu_{n,k} \sum_{k=0}^{n} \sum_{q=1}^{\binom{n}{k}} \left(\varepsilon_{n,k,q}^{X}\right)^2}{\sum_n \mu_{n,k} \sum_{k=0}^{n} \sum_{q=1}^{\binom{n}{k}} \varepsilon_{n,k,q}^{X}} \tag{26}$$

Here $X = DA$ or AD. In order to compute the fraction of molecules that a monomer or oligomer of size n comprises relative to the total number of molecules, we introduce the relative abundance, A_n:

$$A_n = \frac{n\mu_n}{\sum_n n\mu_n} \tag{27}$$

Each value of A_n signifies the fraction of individual molecules which are present in an oligomer of size n, relative to the total number of molecules in the sample, i.e., $\sum_n A_n = 1$. For example, in a mixture comprised of 10 tetramers, 20 dimers, and 40 monomers, the relative abundance of each of the species would be 33.3%.

2.5. Fitting residual for quantifying the difference between theoretical model and computer-simulated data

Fitting of theoretical models to simulated ε_{eff}^{DA}, ε_{eff}^{AD}, or E_{ave} vs X_A datasets was achieved by minimizing a fitting residual, defined here:

$$fitting\ residual = \frac{1}{M}\sum_{m=1}^{M}\frac{\sum_l\left(measured_{l,m}-predicted_{l,m}\right)^2}{\sum_l measured_{l,m}^2} \quad (28)$$

where the summation index l represents X_A values, and the summation index m the different datasets being fitted, i.e., ε_{eff}^{DA}, ε_{eff}^{AD}, or E_{ave} vs X_A. Because up to three datasets were fitted simultaneously in the minimization procedures, the individual components of the residual values were weighted by the sum underneath each respective curve, in order that each dataset contributed equal weight to the combined residual. The sum underneath each curve was used as a weighting factor instead of dividing each term by its variance because the standard deviation of the average RET values was comparatively smaller than those of the two brightness terms, and thereby would "overweight" the fit of the E_{ave} relative to the other two. The smaller standard deviation for the average RET efficiency values is due to the fact that a single brightness point takes hundreds of intensity values to calculate, whereas an RET efficiency value can be calculated for each pixel.

3. Results and discussion

We used Monte-Carlo simulations to generate images mimicking distributions of various sized oligomers comprised of both donor and acceptor molecules. From these images, we were able to construct donor and acceptor intensity distributions, and thereby obtain both RET efficiency and donor/acceptor apparent brightness values, under varying conditions. This allowed us to test whether the formalism developed in the preceding sections for predicting donor and acceptor intensity variations was accurate. Once this was confirmed, we were able to use simulated data to test whether fitting plots of the donor and acceptor molecular brightness and average RET efficiency vs X_A simultaneously added useful constraints to the data interpretation and thereby help to pinpoint the architecture of the underlying sample with greater accuracy, in contrast to traditional analysis procedures which monitor either RET or fluctuations individually.

3.1. Testing the brightness theory using computer-simulated data

We first wanted to confirm the validity of using equation (26) to model the intensity variance for donors and acceptors forming complexes. For this purpose, we used Monte-Carlo simulations to generate fluorescence images from distributions of rhombus shaped tetramers; details on each individual configuration of the rhombic tetramers are listed in Supplementary Figure 1. The simulation protocol is described in Supplementary Note 2. Briefly, a fixed number of tetramers were randomly distributed over matrix elements, or "pixels"; more than one complex was allowed to occupy each pixel. Individual molecules within a complex were assigned either a donor or an acceptor tag randomly, based on a probability computed from the acceptor mole fraction, X_A. Fluorescence intensity values of donors and acceptors were computed for each pixel by summing the counts generated from each individual complex assigned to said pixel. This entire process was repeated for a range of X_A. From the simulated images, we could analyze the fluctuations in both

donor and acceptor intensities and generate plots of ε_{eff}^{DA} and ε_{eff}^{AD} as a function of X_A, as shown by the blue symbols in figure 2. The input parameters used to generate the simulated brightness data were then inserted into equation (26) to calculate values for ε_{eff}^{DA} and ε_{eff}^{AD}; these calculated values are shown by the solid red line in figure 2. As can be seen from the near perfect conformity between the simulated brightness data and the calculated values, the formalism leading to equation (26) for predicting the fluctuations of donor and acceptor intensities appears to be correct.

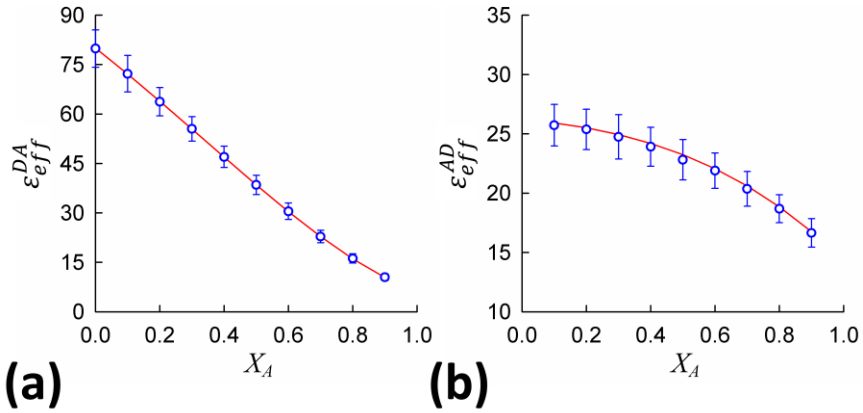

Figure 2. Validation of the formulation used to describe (a) donor and (b) acceptor intensity fluctuations as a function of X_A using computer-simulated images of distributions of tetrameric complexes. Each individual protomer within a tetramer was assigned either a donor or an acceptor identity; this assignment was randomly generated based on probability which was calculated using a fixed acceptor mole fraction value (X_A). Each molecule was randomly distributed over 400 pixels, with an average of 25 protomers/pixel. From each 400-pixel segment, a value of ε_{eff}^{DA} and ε_{eff}^{AD} was extracted. The simulation was performed for a number of X_A values, with 1000 segments generated for each value of X_A. The mean ±SD of ε_{eff}^{DA} and ε_{eff}^{AD} over all segments are shown by the blue symbols with error bars representing ±1 SD. The solid red line is generated by inserting the simulation parameters into equation (26). The exquisite fit of the red line to the data points demonstrates the validity of equation (26) when RET is occurring. Detailed RET efficiency and intensity values for the tetrameric complex are given in Supplementary Figure 1. Additional input parameters to the simulation: $\varepsilon_m^A = 0$, $\varepsilon_m^D = 20$, $E_p = 0.5$, $\sigma_{DET}^2 = 0$, $\gamma = 1$.

Similarly good agreement between the theory and numerical simulations were obtained for dimeric and trimeric complexes, as seen in Supplementary Figure 2.

3.2. Behavior of D and A brightness as a function of model parameters

We next wanted to test how the shape of the plots of the donor and acceptor brightness (i.e., ε_{app}^{DA} and ε_{app}^{AD}, respectively) vs. X_A changed as a function of various model input parameters, including oligomer size, the relative abundance of various oligomer species, and the pairwise RET efficiency, E_p (see reference [25] and Supplementary Note 3 for relation of E_p to intramolecular distances within a protein complex). This exercise unveiled some interesting features in the donor and acceptor brightness vs. X_A plots, suggesting that adding both of these datasets to the analysis of RET data will not be redundant, but restrict the choice of model which accurately predicts measured data and help to better resolve the complexity of the underlying system. In figure 3, both ε_{eff}^{DA} and ε_{eff}^{AD} vs. X_A were plotted for two different oligomer sizes and different values of E_p.

Changes in E_p of course reflect changes in the distances between protomers within the oligomer (see Supplementary Note 3). ε_{eff}^{DA} markedly depends on X_A, following a straight line at low E_p values and becoming more nonlinear as E_p increases. This is in stark contrast to the behavior of the average RET efficiency vs. X_A plots computed for the dimer only model (Supplementary Figure 3a), which steadily increase as a function of E_p.

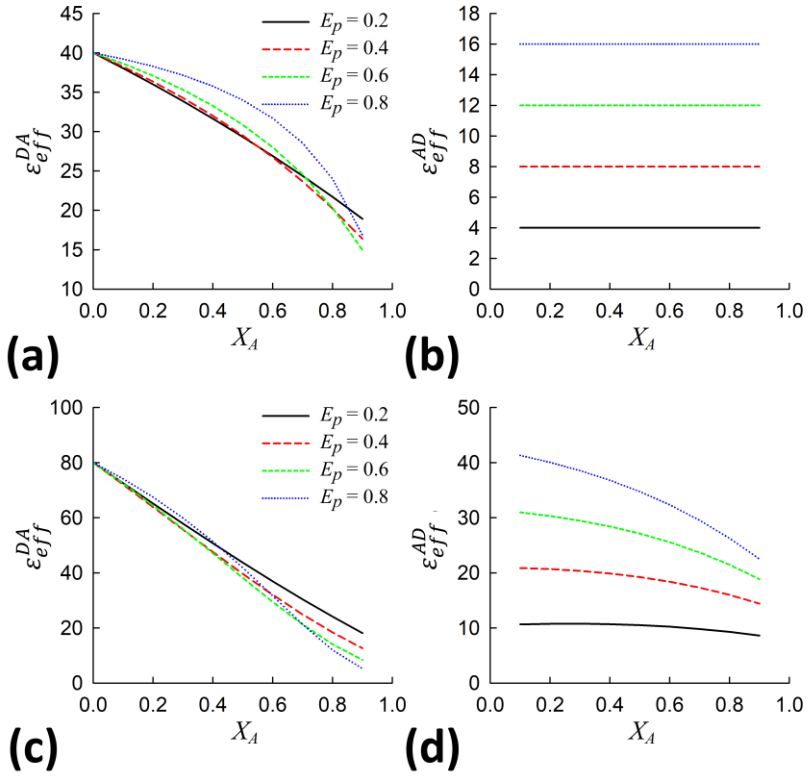

Figure 3. Apparent brightness of donor, ε_{eff}^{DA}, and acceptor, ε_{eff}^{AD}, vs. acceptor mole fraction, X_A, as determined from equation (26) for (a-b) dimers (n = 2) and (c-d) rhombus shaped tetramers (n = 4). The plots were generated for four different values of the pairwise RET efficiency, E_p, in order to illustrate the dependence of the curvature on the level of RET efficiency occurring in the complex. As is evident in (b), the value of ε_{eff}^{AD} is uniquely determined by E_p for the case of dimers; this quantity is completely unaffected by changes in the dimer/monomer concentration ratio, as is seen in figure 4b.

As for the behavior of ε_{eff}^{AD}, it is seen from figure 3(b) that it presents no dependence on X_A for the case of pure dimers. This behavior can be explained by first noting that the monomeric acceptor brightness, ε_m^A, used in computing this plot was set to zero, which represents a situation where there is no direct excitation of the acceptor molecules with laser light. In this case, only the DA and AD configurations of the dimers, which are identical with regard to fluorescence properties, would generate acceptor signal. Therefore, there is actually only one species present which contributes to the acceptor signal. Any dependence of ε_{eff}^{AD} on X_A would be caused by a change in the proportion of various oligomer configurations, i.e., $\mu_{n,k}$ of equation (24), as the ratio of donor to acceptor concentration changes. However, since the DD and AA molecules contribute nothing to the acceptor signal, this change in number is not reflected in the calculation of ε_{eff}^{AD}, hence the constant ε_{eff}^{AD} value over the entire X_A range. By contrast, ε_{eff}^{AD} is linearly dependent on E_p (see figure 3b), which provides an exquisite means for determining the true value of E_p from

experiments. For larger oligomeric complexes, plots of ε_{eff}^{AD} vs. X_A acquire significant curvature, because more than one oligomer configuration now contributes to the acceptor fluorescence signal (see figure 3d). The plots of ε_{eff}^{AD} vs X_A still resolve different E_p values quite clearly, as long as there are some donors in the system, i.e., for $X_A < 1$.

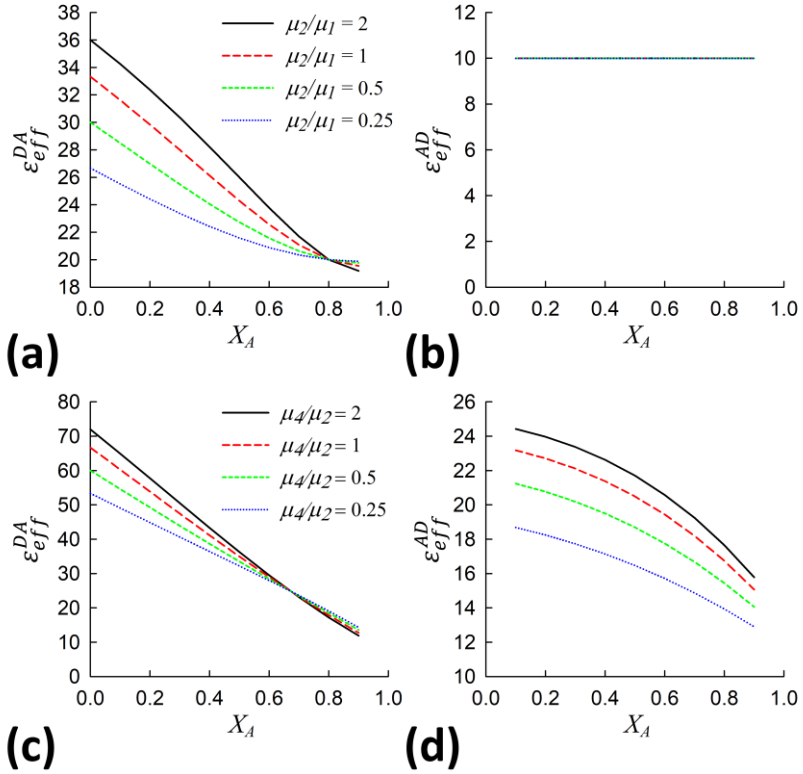

Figure 4. Apparent brightness values of donor, ε_{eff}^{DA}, and acceptor, ε_{eff}^{AD}, vs. acceptor mole fraction, X_A, as determined from equation (26) for various ratios between: (a), (b) dimer and monomer concentrations and (c), (d) tetramer and dimer concentrations. The concentration ratio of the various oligomer species affects the plots in different manners. As is evident in (b), the ε_{eff}^{AD} shape is completely unaffected by changes in the dimer/monomer concentration ratio, while variation in the concentration ratio of the oligomer species strongly modulates the value of the *y*-intercept in (a) and (c).

Figure 4 illustrates the behavior of the brightness vs. X_A plots for a mixture of monomers and dimers (panels a and b) as well as mixture of dimers and tetramers (panels c and d), as the concentration of the two species comprising the mixture is varied. As can be seen, ε_{app}^{AD} is completely unaffected by changes in the dimer/monomer concentration ratio. This is due to the fact that, when $\varepsilon_m^A = 0$, the monomeric acceptors contribute nothing to the fluctuations in acceptor signal, as the acceptors are not directly excited by light. In contrast, a change in concentration ratio between the two species induces a strong change in the *y*-intercept of the ε_{app}^{DA} plot, as seen in figures 4(a) and 4(c) for both mixtures, as well as a change in the relative disposition along the *y*-axis of the ε_{app}^{AD} vs. X_A plots.

By combining the qualitative features illustrated in figures 3 and 4, one can easily envision how simultaneously fitting donor and acceptor brightness vs. X_A plots would help pinpoint the correct structural model for mixtures of various oligomer sizes with unknown relative abundance

and structural properties and provide the correct parameters of the model. The *y*-intercept of the ε_{eff}^{DA} plot is the dominant contributor to resolving the relative abundance of each of the oligomer species, while the ε_{eff}^{AD} helps to "lock in" the correct value of E_p, the dominant parameter related to the distances between protomers within the oligomer model being considered.

3.3. Resolving mixtures of monomers and dimers using iFRET

We next set out to determine whether the size and geometrical characteristics of the oligomers may be extracted from numerically simulated donor and acceptor brightness vs. X_A plots using the theory described in section 2.4. For this purpose, we generated simulated brightness and RET efficiency data from mixtures of monomers and dimers (figure 5) as well as monomers/dimers/tetramers (figure 6) of the average RET efficiency, E_{ave}, and donor/acceptor molecular brightness, ε_{eff}^{DA} and ε_{eff}^{AD}, as a function of X_A. Each of the simulated data sets was fitted, both individually and globally, with the equations predicting these quantities theoretically (equations S2 and 26). The global analysis of the multi-parameter dataset, a procedure for which we have coined the term iFRET in this paper, signifies that a common set of parameters is used to generate a theoretical prediction for the structural oligomeric models from brightness and RET efficiency data.

Knowing the input parameters used to generate the data, we were interested to see if fitting of the simulated data could return these known values. Furthermore, we were also interested in how "tightly" we could determine the best-fit parameters. To this end, we employed an iterative fitting process, the results of which are shown in figures 5(d-e) and 6(a), to help assess how unique the best-fit parameters were. To construct the plots shown in figures 5(d-e) and 6(a), one fitting parameter, e.g., E_p, was first set to a fixed value, and all other parameters were adjusted until the difference between the simulated brightness and RET efficiency data and theoretically predicted curves, quantified by the fitting residual given in Equation (28), was minimized. Then, E_p was increased by a small increment, and the fitting procedure involving the other parameters was run again.

Figure 5 illustrates the result of applying the minimization procedure to data extracted from computer-generated images containing mixtures of dimers and monomers. The relative abundance values used to generate the images were $A_2 = 0.667$ for the dimers and $A_1 = 0.333$ for the monomers, while the pairwise RET efficiency was set to $E_p = 0.5$. The fitting residuals obtained by fitting ε_{eff}^{DA}, ε_{eff}^{AD}, or E_p vs. X_A curves individually are shown using plots with filled symbols (see panels d and e in figure 5); in these cases, the fitting residual was defined so that it only included the "measured" (i.e., simulated) and theoretical terms from one of the ε_{eff}^{DA}, ε_{eff}^{AD}, or E_{ave} vs. X_A plots ($M = 1$ in Equation 28). Figure 5d shows that any E_p can be used to fit the individual ε_{eff}^{DA} and E_{ave} vs X_A plots, simply by adjusting the relative abundance values of the monomers and dimers to compensate for discrepancies between the theoretical and measured curves caused by varying the value of E_p. Conversely, fitting only the ε_{app}^{AD} vs. X_A curve does not reveal unique information regarding the relative abundances of the two species, as the same exact fit is achieved regardless of A_2/A_1 value, as seen in figure 5e. We were never able to extract both the RET

efficiency and the relative abundance information (values of A_1 and A_2) from the fitting of ε_{eff}^{DA}, ε_{eff}^{AD}, or E_{ave} vs X_A curves individually (i.e., $M = 1$ in equation 28); we need to be able to fix either E_p or A_2/A_1 during the fitting. When ε_{eff}^{DA} and E_{ave} vs X_A curves are fitted simultaneously (i.e., $M = 2$ in equation 28), the "tightness" of the fitting residual vs. E_p plot (green squares in figures 5d) improves slightly, although the curvature is still somewhat shallow.

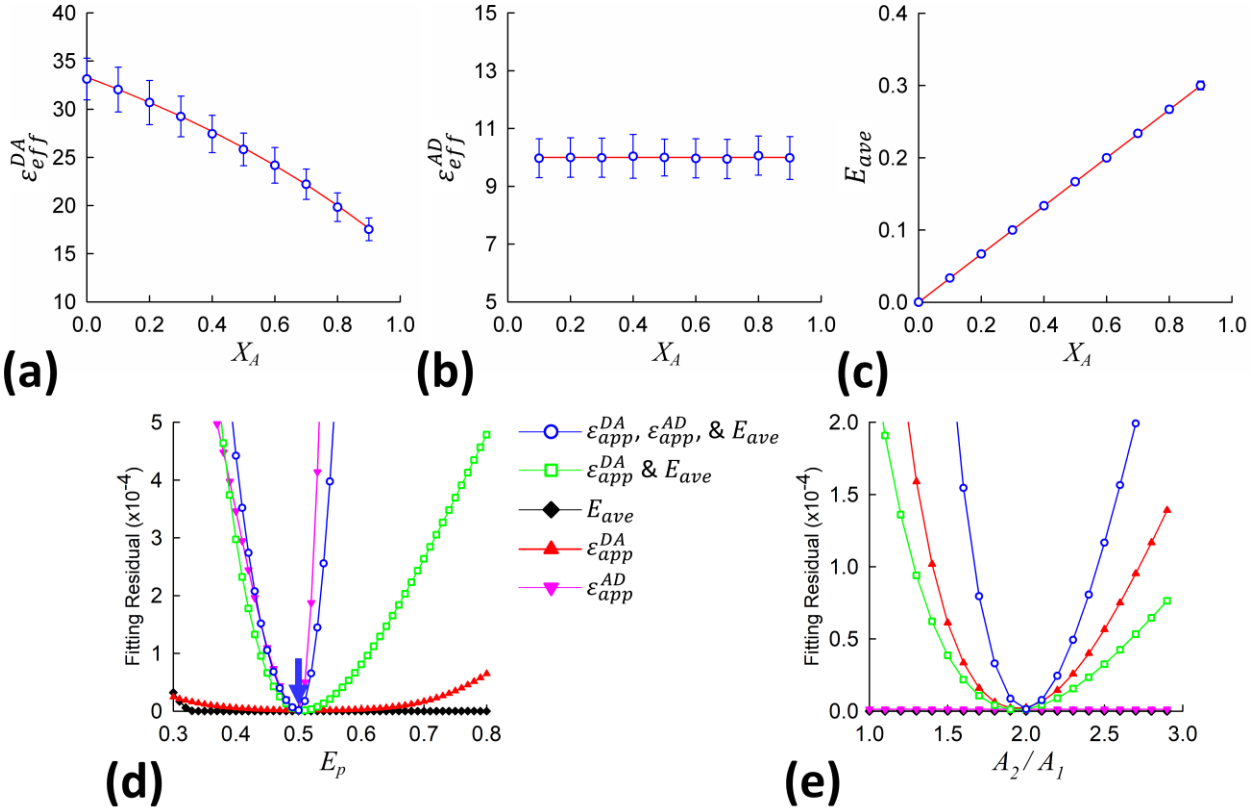

Figure 5. Simultaneous fitting of the average ε_{eff}^{DA}, ε_{eff}^{AD}, and E_{ave} values extracted from a Monte-Carlo simulated mixture of monomers and dimers with relative abundances A_2=0.667, and A_1=0.333 and a pairwise RET efficiency in the dimer of E_p=0.5. Each molecule was randomly distributed over a 400-pixel segment with an average of 25 protomers/pixel. From each 400pixel segment, a value of ε_{eff}^{DA}, ε_{eff}^{AD}, and E_{ave} was extracted. The simulation was performed for a number of X_A values, with 300 segments generated for each value of X_A. The mean values of (a) ε_{eff}^{DA} (b) ε_{eff}^{AD} and (c) E_{ave} , represented by blue symbols, were obtained by averaging over the 300 segments for each X_A value; error bars denote ±1 SD. The red line represents the result of simultaneously fitting the brightness and RET efficiency simulated data sets using equations (26) and (S2). The best fit was obtained when using a pairwise RET efficiency value of E_p=0.5 and relative abundance values of: A_4=0, A_2=0.667, and A_1=0.333, exactly equal to the input parameters to the simulation. (d)-(e) Plots comparing the uniqueness of the best fit parameters by defining the fitting residual to incorporate one, two, or all three of the ε_{eff}^{DA}, ε_{eff}^{DA}, and E_{ave} vs. X_A data: ε_{eff}^{DA} only (red triangles), ε_{eff}^{AD} only (pink triangles), E_{ave} only (black diamonds), ε_{eff}^{DA} and E_{ave} (green squares), or ε_{eff}^{DA} , ε_{eff}^{AD}, and E_{ave} (blue circles). For each of the plots, either the parameter (d) E_p or (e) A_2/A_1 was held fixed and the other parameters altered until the lowest residual was achieved; each point in the plots represents the fitting residual value plotted against the corresponding value of the fixed parameter. The fitting procedure which incorporated all three datasets (blue circles) clearly achieved the sharpest minimum. The parameters extracted from the point indicated by the blue arrow in (d) were used to generate the red lines of (a-c).

Finally, the minimization procedure was performed when incorporating all three of the ε_{eff}^{DA}, ε_{eff}^{AD}, or E_{ave} vs X_A datasets into the fitting residual (i.e., $M = 3$ in equation 28). The minima of the fitting residual vs. E_p (figure 5, panel d) or A_2/A_1 (figure 5, panel e) resulting from the three-component residual (blue open symbols) are very well defined, and the extracted fitting parameters match exactly those used for generating the computer-simulated brightness and RET efficiency data. It is evident from figure 5 (panels d and e) that the plots of ε_{eff}^{DA}, ε_{eff}^{AD}, and E_{ave} vs X_A all must be included in the minimization procedure to fully realize the potential of iFRET. What is even more encouraging is the fact that we added more complexity to the model used to fit the simulated brightness and RET efficiency data, in the form of a third oligomer size ($n = 4$), and still obtained the correct input parameters.

3.4. Identification of structural models for higher order oligomers from computer-simulated data

We next wanted to gauge the power of this approach by applying it to an even more complicated mixture of molecules. Therefore, we added rhombus shaped tetramers to a mixture of monomers and dimers ($A_4 = 0.250$, $A_2 = 0.400$, $A_1 = 0.350$) and again generated computer-simulated datasets for the donor/acceptor molecular brightness and average RET efficiency (figures 6a-c). The mixture of monomers, dimers and tetramers considered above is relevant to situations where each protomer has two binding sites with very different binding affinities. Details on all of the different rhombus tetramer configurations are listed in Supplementary Figure 1. Multiple iterative fitting procedures were performed using individual ε_{eff}^{DA}, ε_{eff}^{AD}, and E_{ave} vs X_A curves as well as combinations of them, and once again, as is evident in figure 6(d), the most restrictive fitting process occurred when incorporating all three. Reassuringly, the best-fit parameters extracted from the three-component residual fitting, A_4=0.243, A_2=0.409, and A_1=0.347, matched extremely well the value of the input parameters. An additional computer simulated dataset was generated from mixtures which incorporated trimer complexes in addition to monomers, dimers and tetramers (Supplementary Figure 4). Similarly good agreement was found between the input and the best-fit parameters extracted from analysis of the simulated data generated from the mixture which incorporated trimers as well.

The main critique one could raise regarding our analysis presented above of the mixture incorporating tetramers is that the correct model for the tetramer was known beforehand. We will illustrate next how effective this approach is when neither the oligomer size nor its structure is known a priori. We tested a variety of models on the simulated brightness and RET efficiency data shown in figure 6, which was generated using a mixture of monomers, dimers, and rhombus shaped tetramers. All of the oligomer models tested are shown in figure 7(a). Fitting residual vs. E_p plots have been prepared for each type of model (figure 7b) in order to see if a global minimum could be achieved across the various models tested. We considered the worst-case scenario for a model identification task, in which the number of fitting parameters was the same for each model tested; this means that the polygons which were tested all had sides of equal length (equilateral triangle, rhombus, and square) and this side length was the same as the distance between fluorophores for the geometries possessing linear arrangements. Furthermore, the acute angle describing rhombus

model was held fixed (α = 60º) during the fitting process. Keeping the number of fitting parameters constant enabled a direct comparison between the resulting residual values from fitting each model. As seen in figure 7(b), the Fitting Residual vs. E_p plot for the correct model, the rhombus shaped tetramer, provided by far the lowest minimum fitting residual of all the oligomer types tested. The minimum fitting residual for the correct model, the rhombus, was 20-fold lower than the next best fitting model, the square tetramer, providing unambiguous identification of the former as the correct oligomer structure.

Additional tests were performed to evaluate how precisely detailed geometrical parameters describing a more arbitrarily shaped tetramer could be determined using iFRET. Simulated images were generated from mixtures of monomers, dimers and a parallelogram shaped tetramer whose side lengths were not equal (as opposed to the more ideal shapes shown in Fig. 7a). The geometrical parameters needed to describe the parallelogram are illustrated in Supplementary Figure 5. Fitting of the simulated data was performed with two additional fitting parameters included in the process: the acute angle, α, and the ratio of the lengths of the sides, r_2/r_1, of the parallelogram. Even with the additional fitting parameters needed to describe the more complicated shape of the oligomer, the relative abundance values determined closely matched the input values. In addition, the parameters α and r_2/r_1 which describing the shape of the parallelogram also closely matched those of the oligomer used to generate the simulated data (See Supplementary Note 4 and Supplementary Tables 1 and 2).

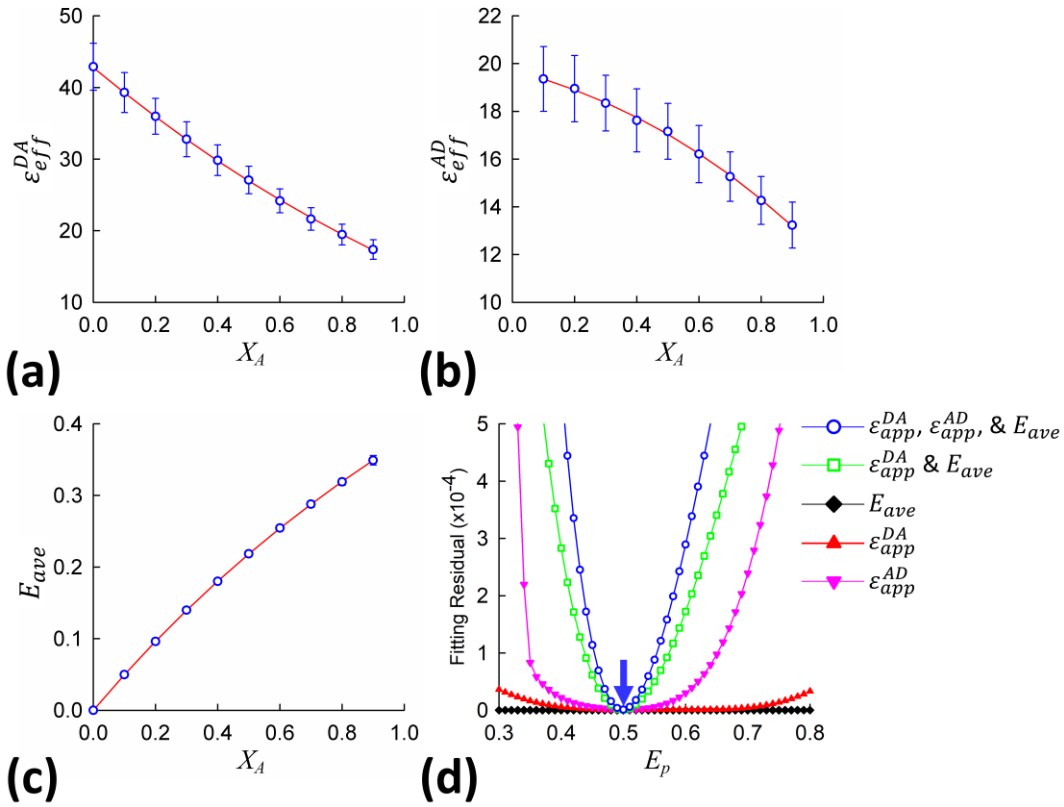

Figure 6. Simultaneous fitting of the average ε_{eff}^{DA}, ε_{eff}^{AD}, and E_{ave} values extracted from a Monte-Carlo simulated mixture of monomers, dimers, and tetramers with relative abundances: A_4=0.250, A_2=0.400, and A_1=0.350 and pairwise RET efficiency E_p=0.5. Each molecule was randomly distributed over a 400 pixel segment with an average of 25 protomers/pixel. From each 400 pixel segment, a value of ε_{eff}^{DA}, ε_{eff}^{AD}, and E_{ave} was extracted. The simulation was performed for a number of X_A values, with 300 segments generated for each value of X_A. The mean values of (a) ε_{eff}^{DA} (b) ε_{eff}^{AD} and (c) E_{ave}, represented by blue symbols, were obtained by averaging over the 300 segments for each X_A value; error bars denote ±1 SD. The red line represents the result of simultaneously fitting the brightness and RET efficiency simulated data sets using equations (26) and (S2). The best fit was obtained when using a pairwise RET efficiency value of E_p=0.5 and relative abundance values: A_4 = 0.243, A_2 = 0.405, and A_1 = 0.349. (d) Comparison of fitting residual vs. E_p plots when one, two, or all three of ε_{eff}^{DA}, ε_{eff}^{AD}, and E_{ave} vs. X_A data were included in the fitting residual: ε_{eff}^{DA} only (red triangles), ε_{eff}^{AD} only (pink triangles), E_{ave} only (black diamonds), ε_{eff}^{DA} and E_{ave} (green squares), or ε_{eff}^{DA}, ε_{eff}^{AD}, and E_{ave} (blue circles). For each plot, the parameter E_p was held fixed and the relative abundance parameters altered until the lowest fitting residual was achieved; each point in the plots represents the residual value plotted against the corresponding value for E_p used to achieve it. The fitting procedure which incorporated all three datasets (blue circles) clearly achieved the sharpest minimum. The parameters extracted from the point indicated by the blue arrow were used to generate the red lines of (a-c).

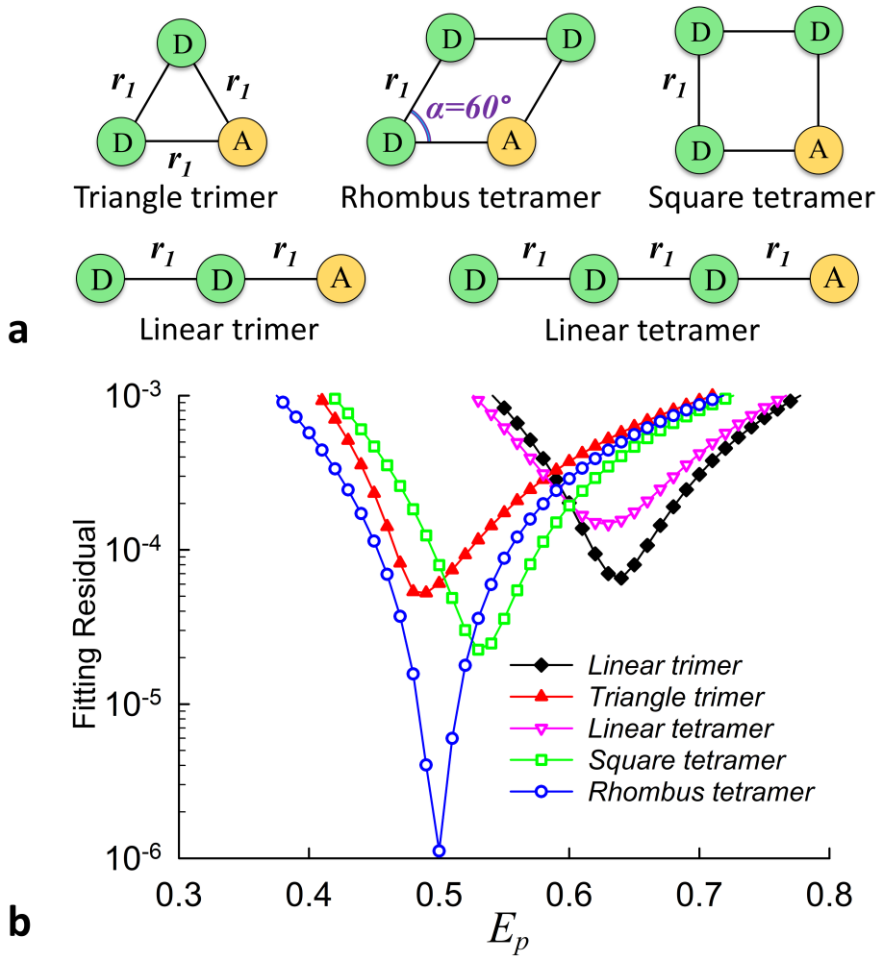

Figure 7. (a) Geometrical depiction of various oligomer structure models used for fitting the data shown in figure 6. **(b)** Fitting residual vs. E_p plots obtained after applying the various oligomer models shown in (a) to simulated ε_{eff}^{DA}, ε_{eff}^{AD}, and E_{ave} vs. X_A plots. A clear minimum of the fitting residual is seen for the correct quaternary structure model, the rhombus shaped tetramer with acute angle of 60° and E_p = 0.5. Furthermore, the correct relative abundance values

were also extracted using this model. The minimum fitting residual values for each of the oligomers tested are: 5.9×10^{-5} for the linear trimer, 4.7×10^{-5} for the triangle trimer, 1.3×10^{-4} for the linear tetramer, 2.0×10^{-5} for the square tetramer, and as low as 1.1×10^{-6} for the rhombus tetramer.

3.5. Testing iFRET from simulated data incorporating actual detector noise

One potential challenge faced not only by iFRET but also by any fluorescence-based detection technique, including other RET-based and FFS-based techniques, is a dearth of photons at the extremities of the X_A intervals under certain experimental conditions. For example, if the concentration of molecules is very low, and the direct excitation of the acceptor by the laser is negligible, then the amount of acceptor signal reaching the detector will be scarce for both low and high values of X_A. For low signal levels, it is possible that the extraction of parameters from the ε_{eff}^{DA}, ε_{eff}^{AD}, and E_{ave} vs X_A datasets would become unreliable due to sources of noise typically found in fluorescence measurements. Therefore, we performed simulations to assess the effect of noise originating, from the charge amplification process in a cooled electron-multiplying CCD (EMCCD) camera, on the uniqueness of the parameter values extracted from the ε_{eff}^{DA}, ε_{eff}^{AD}, and E_{ave} vs. X_A plots. To add noise to the simulated brightness and RET efficiency data, the photon count was tallied for a particular pixel, and then run through a signal amplification process (see Supplementary Note 5 for more details). The noise characteristics of the signal amplification (Supplementary Figure 6) were measured using a constant light source and an electron-multiplying CCD (EMCCD) camera (iXon Ultra 897, Andor Technologies, Belfast, UK).

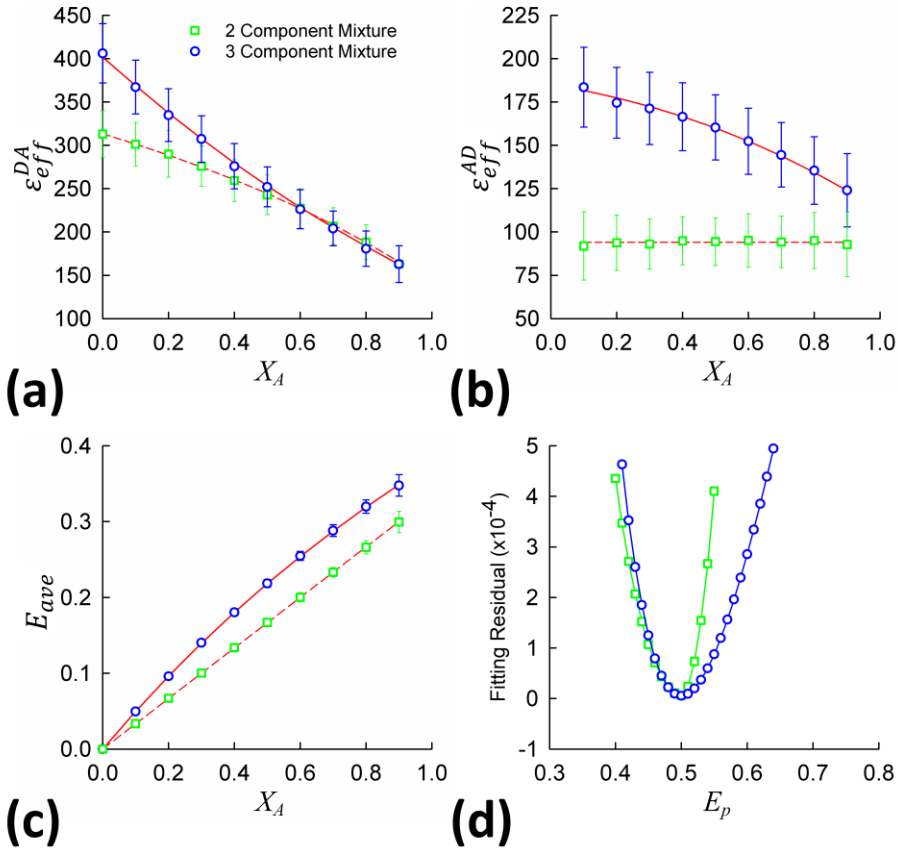

Figure 8. a-c. Incorporation of EMCCD gain noise to Monte-Carlo simulations of various monomer, dimer, and tetramer mixtures. Molecules were distributed over 400-pixel segments at an average of 25 protomers/pixel. The intensity values from each pixel were computed, and then run through a charge amplification process (see Supplementary Note 5), to obtain an output intensity. From each 400-pixel segment, a value of ε_{eff}^{DA}, ε_{eff}^{AD}, and E_{ave} was extracted from the EM Gain amplified intensities. The mean ±1 SD of (a) ε_{eff}^{DA} (b) ε_{eff}^{AD} and (c) E_{ave} , represented by blue circles for a three component mixture consisting of monomers, dimers and tetramers (A_4=0.250, A_2=0.400, and A_1=0.350), and green squares for a two component mixture consisting of monomers and dimers (A_4=0, A_2=0.667, and A_1=0.333), were obtained by averaging over the 300 segments for each X_A value. The red line represents the result of simultaneously fitting the brightness and RET efficiency simulated data sets using equations (26) and (S2). **d.** Plots displaying the uniqueness of the best fit relative abundance and E_p fitting parameters. A clear minimum is established for both simulations at the input value of E_p=0.5, even in the presence of detector noise. Best-fit relative abundance parameters for each of the simulations are given in Table 1.

Simulations with EM gain amplification, and the associated noise factor, applied to photon counts were executed (see Table 1) for a mixture of monomers and dimers (see 2-Component Mixture heading in Table 1) as well as one incorporating rhombus shaped tetramers (3-Component Mixture heading), with the results shown in figure 8. While the error bars on the data points in each of the ε_{eff}^{DA}, ε_{eff}^{AD}, and E_{ave} vs. X_A plots increased slightly, highly convergent fittings and accurate parameter extraction were still achieved, as can be seen in the fitting residual vs. E_p plots of figure 8(d) as well as from the comparison of input parameters used in computer simulations and the parameters extracted from data fitting, all of which are given in Table 1.

Table 1. Comparison between the input parameters used for computer simulations of the data shown in Figure 8 and the best-fit parameters obtained from fitting equations (S2) and (26). Simulations were performed for mixtures incorporating monomers and dimers (2-Component Mixture) and monomers, dimers and tetramers (3-Component Mixture). The simulated data were fit using a total of seven adjustable parameters in the fitting procedure: α, r_2/r_1, E_p, as well as the relative abundance values of tetramers, trimers, dimers, and monomers (i.e., A_4 , A_3, A_2 and A_1).

	2-Component Mixture		3-Component Mixture	
Parameter	Simulations Input	Best-Fit Results	Simulations Input	Best-Fit Results
E_p	0.500	0.499	0.500	0.501
α (^{0})	-	-	60.0	60.5
r_2/r_1	-	-	1.00	1.00
A_4	0.000	0.001	0.250	0.220
A_3	0.000	0.000	0.000	0.057
A_2	0.667	0.666	0.400	0.364
A_1	0.333	0.333	0.350	0.360

4. Conclusion

FFS and RET are powerful techniques which have been vital to protein-protein interaction studies for the past three or four decades. However, when applied individually, both face challenges when it comes to describing the complex picture of membrane receptors self-associating or associating with other receptors to form oligomers. As we mentioned above, analysis of intensity fluctuations provides stoichiometric information about protein complexes but gives no information regarding their quaternary structure. Conversely, RET is ideally suited to measure intramolecular distances between protein subunits in a complex, and hence can deliver information on the proteins quaternary structure. However, when the proteins of interest form an equilibrium of multiple sized oligomers, knowledge regarding the relative abundances of the various oligomer sizes is needed to properly interpret the fluorescence data, otherwise multiple models can fit the data equally well.

We showed in this report that combining these two complementary techniques within a method, for which we have coined the term iFRET, helps restrict the choice of models which accurately predict the measured fluorescence data and leads to a more accurate quantification of the interactions of the underlying system. Because of the unique dependence of both the RET efficiency and intensity fluctuations on the ratio of donors to acceptors in the sample, adding measurements at various X_A values further constrains the data fitting process and thereby increases the reliability of the best-fit parameter values. Using a global analysis procedure to simultaneously fit both RET and donor and acceptor intensity fluctuation data, we have demonstrated the remarkable ability of iFRET to accurately determine the relative abundance as well as the quaternary structure of the protein oligomer complexes comprising a mixture of monomers, dimers, and tetramers.

iFRET may be used to study the interactions of a variety of membrane receptors, including G protein-coupled receptors, receptor tyrosine kinases, and ligand-gated ion channels, as long as the protein of interest can be labeled with pairs of fluorescent proteins. The method should be implementable over a wide range of receptor concentrations, which allows for the compilation of oligomerization binding curves, represented by the relative abundance of a particular oligomer size as a function of the total concentration of molecules. From these binding curves, the association/dissociation constants characterizing not only the equilibrium between monomers and dimers, but also the equilibrium between dimers and higher order oligomers can be determined. In addition to the equilibrium constants, the geometrical parameters of the oligomers may be determined using iFRET. Changes in the equilibrium constants and/or geometrical parameters of the oligomers may be probed after treating the receptors with various agonists, antagonists, and inverse agonists. Therefore, we believe the wealth of information resulting from the application of iFRET could potentially provide insight into the functional significance of receptor oligomerization in living cells and the extent to which this organization is influenced by that of ligand binding.

Acknowledgments

This work was partly supported by grants from the National Science Foundation (grant numbers PHY-1126386 and DBI-1919670) as well as the UWM Research Growth Initiative (101X396) awarded to V.R. The authors have declared that no conflicting interests exist.

References

[1] Palczewski K 2010 Oligomeric forms of G protein-coupled receptors (GPCRs). *Trends Biochem. Sci.* **35** 595-600.

[2] Farran B 2017 An update on the physiological and therapeutic relevance of GPCR oligomers. *Pharmacol. Res.* **117** 303-327.

[3] Milligan G, Ward RJ, and Marsango S 2019 GPCR homo-oligomerization. *Curr. Opin. Cell Biol.* **57** 40-47.

[4] Selvin PR 2000 The renaissance of fluorescence resonance energy transfer. *Nat. Struct. Mol. Biol.* **7** 730-4.

[5] Piston DW and Kremers GJ 2007 Fluorescent protein FRET: the good, the bad and the ugly. *Trends Biochem. Sci.* **32** 407-414.

[6] Sahoo H 2011 Forster resonance energy transfer - A spectroscopic nanoruler: Principle and applications. *Journal of Photochemistry and Photobiology C-Photochemistry Reviews* **12** 20-30.

[7] Lakowicz JR, *Principles of Fluorescence Spectroscopy*. 3rd ed. 2006, Berlin: Springer.

[8] Clegg RM, *Fluorescence resonance energy transfer*, in *Fluorescence Imaging Spectroscopy and Microscopy*, X.F. Wang and B. Herman, Editors. 1996, Wiley: New York. p. 179-252.

[9] Jares-Erijman EA and Jovin TM 2003 FRET imaging. *Nat. Biotechnol.* **21** 1387-1395.

[10] Elson EL 2011 Fluorescence Correlation Spectroscopy: Past, Present, Future. *Biophys. J.* **101** 2855-2870.

[11] Jameson DM, Ross JA, and Albanesi JP 2009 Fluorescence fluctuation spectroscopy: ushering in a new age of enlightenment for cellular dynamics. *Biophys. Rev.* **1** 105-118.

[12] Ries J and Schwille P 2012 Fluorescence correlation spectroscopy. *Bioessays* **34** 361-368.

[13] Digman MA and Gratton E 2011 Lessons in Fluctuation Correlation Spectroscopy. *Annual Review of Physical Chemistry, Vol 62* **62** 645-668.

[14] Valeur B and Berberan-Santos MN, *Molecular Fluorescence: Principles and Applications* 2nd ed. 2012, Weinheim: Wiley-VCH.

[15] Förster T 1948 Zwischenmolekulare Energiewanderung und Fluoreszenz. *Annalen der Physik* **2** 55-75.

[16] King C, Stoneman M, Raicu V, and Hristova K 2016 Fully quantified spectral imaging reveals in vivo membrane protein interactions. *Integrative Biology* **8** 216-229.

[17] Chen LR, Novicky L, Merzlyakov M, Hristov T, and Hristova K 2010 Measuring the Energetics of Membrane Protein Dimerization in Mammalian Membranes. *J. Am. Chem. Soc.* **132** 3628-3635.

[18] Singh DR, Kanvinde P, King C, Pasquale EB, and Hristova K 2018 The EphA2 receptor is activated through induction of distinct, ligand-dependent oligomeric structures. *Communications Biology* **1** 1-12.

[19] Maurel D*, et al.* 2008 Cell-surface protein-protein interaction analysis with time-resolved FRET and snap-tag technologies: application to GPCR oligomerization. *Nat Methods* **5** 561-7.

[20] Albizu L*, et al.* 2010 Time-resolved FRET between GPCR ligands reveals oligomers in native tissues. *Nat. Chem. Biol.* **6** 587-594.
[21] King C, Wirth D, Workman S, and Hristova K 2018 Interactions between NRP1 and VEGFR2 molecules in the plasma membrane. *Biochimica Et Biophysica Acta-Biomembranes* **1860** 2118-2125.
[22] King C and Hristova K 2019 Direct measurements of VEGF-VEGFR2 binding affinities reveal the coupling between ligand binding and receptor dimerization. *J. Biol. Chem.* **294** 9064-9075.
[23] Raicu V, Stoneman MR, Fung R, Melnichuk M, Jansma DB, Pisterzi LF, Rath S, Fox M, Wells JW, and Saldin DK 2009 Determination of supramolecular structure and spatial distribution of protein complexes in living cells. *Nature Photonics* **3** 107-113.
[24] Raicu V and Singh DR 2013 FRET Spectrometry: A New Tool for the Determination of Protein Quaternary Structure in Living Cells. *Biophys. J.* **105** 1937-1945.
[25] Mishra AK, Gragg M, Stoneman MR, Biener G, Oliver JA, Miszta P, Filipek S, Raicu V, and Park PSH 2016 Quaternary structures of opsin in live cells revealed by FRET spectrometry. *Biochem. J.* **473** 3819-3836.
[26] Patowary S, Alvarez-Curto E, Xu TR, Holz JD, Oliver JA, Milligan G, and Raicu V 2013 The Muscarinic M3 Acetylcholine receptor exists as two differently sized complexes at the plasma membrane. *Biochem. J.* **452** 303-312.
[27] Schmidt S, Jakab M, Costa I, Furst J, Ravasio A, Paulmichl M, Botta G, and Ritter M 2009 Quaternary Structure Assessment of ICln by Fluorescence Resonance Energy Transfer (FRET) in vivo. *Cell. Physiol. Biochem.* **23** 397-406.
[28] Raicu V, Jansma DB, Miller RJ, and Friesen JD 2005 Protein interaction quantified in vivo by spectrally resolved fluorescence resonance energy transfer. *Biochem. J.* **385** 265-77.
[29] Stoneman MR, Paprocki JD, Biener G, Yokoi K, Shevade A, Kuchin S, and Raicu V 2017 Quaternary structure of the yeast pheromone receptor Ste2 in living cells. *Biochimica Et Biophysica Acta-Biomembranes* **1859** 1456-1464.
[30] Li M, Reddy LG, Bennett R, Silva ND, Jones LR, and Thomas DD 1999 A fluorescence energy transfer method for analyzing protein oligomeric structure: Application to phospholamban. *Biophys. J.* **76** 2587-2599.
[31] Woehler A, Wlodarczyk J, and Ponimaskin EG 2009 Specific oligomerization of the 5-HT1A receptor in the plasma membrane. *Glycoconj. J.* **26** 749-756.
[32] King C, Raicu V, and Hristova K 2017 Understanding the FRET Signatures of Interacting Membrane Proteins. *J. Biol. Chem.* **292** 5291-5310.
[33] Raicu V 2019 Ab Initio Derivation of the FRET Equations Resolves Old Puzzles and Suggests Measurement Strategies. *Biophys. J.* **116** 1313-1327.
[34] Raicu V 2007 Efficiency of resonance energy transfer in homo-oligomeric complexes of proteins. *J. Biol. Phys.* **33** 109-127.
[35] Singh DR, Mohammad MM, Patowary S, Stoneman MR, Oliver JA, Movileanu L, and Raicu V 2013 Determination of the quaternary structure of a bacterial ATP-binding cassette (ABC) transporter in living cells. *Integrative Biology* **5** 312-323.
[36] Singh DR and Raicu V 2010 Comparison between whole distribution- and average-based approaches to the determination of fluorescence resonance energy transfer efficiency in ensembles of proteins in living cells. *Biophys. J.* **98** 2127-2135.

[37] Raicu V 2018 Extraction of information on macromolecular interactions from fluorescence micro-spectroscopy measurements in the presence and absence of FRET. *Spectrochimica Acta Part a-Molecular and Biomolecular Spectroscopy* **199** 340-348.
[38] Bag N and Wohland T 2014 Imaging Fluorescence Fluctuation Spectroscopy: New Tools for Quantitative Bioimaging. *Annual Review of Physical Chemistry, Vol 65* **65** 225-248.
[39] Raicu V and Schmidt WF, *Advanced Microscopy Techniques*, in *G-Protein-Coupled Receptor Dimers*, K. Herrick-Davis, G. Milligan, and G. Di Giovanni, Editors. 2017. p. 39-75.
[40] Anthony NR and Berland KM 2014 tau FCS: Multi-Method Global Analysis Enhances Resolution and Sensitivity in Fluorescence Fluctuation Measurements. *PLoS One* **9**.
[41] Felekyan S, Sanabria H, Kalinin S, Kuhnemuth R, and Seidel CAM 2013 Analyzing Forster Resonance Energy Transfer with Fluctuation Algorithms. *Fluorescence Fluctuation Spectroscopy (Ffs), Pt B* **519** 39-85.
[42] Chen Y, Muller JD, So PT, and Gratton E 1999 The photon counting histogram in fluorescence fluctuation spectroscopy. *Biophys. J.* **77** 553-67.
[43] Digman MA, Dalal R, Horwitz AF, and Gratton E 2008 Mapping the number of molecules and brightness in the laser scanning microscope. *Biophys. J.* **94** 2320-32.
[44] Kask P, Palo K, Ullmann D, and Gall K 1999 Fluorescence-intensity distribution analysis and its application in biomolecular detection technology. *Proc. Natl. Acad. Sci. U. S. A.* **96** 13756-13761.
[45] Godin AG, Costantino S, Lorenzo LE, Swift JL, Sergeev M, Ribeiro-da-Silva A, De Koninck Y, and Wiseman PW 2011 Revealing protein oligomerization and densities in situ using spatial intensity distribution analysis. *Proc. Natl. Acad. Sci. U. S. A.* **108** 7010-7015.
[46] Qian H and Elson EL 1990 On the Analysis of High-Order Moments of Fluorescence Fluctuations. *Biophys. J.* **57** 375-380.
[47] Digman MA, Wiseman PW, Choi C, Horwitz AR, and Gratton E 2009 Stoichiometry of molecular complexes at adhesions in living cells. *Proc. Natl. Acad. Sci. U. S. A.* **106** 2170-2175.
[48] Godin AG, Rappaz B, Potvin-Trottier L, Kennedy TE, De Koninck Y, and Wisemant PW 2015 Spatial Intensity Distribution Analysis Reveals Abnormal Oligomerization of Proteins in Single Cells. *Biophys. J.* **109** 710-721.
[49] Pediani JD, Ward RJ, Marsango S, and Milligan G 2018 Spatial Intensity Distribution Analysis: Studies of G Protein-Coupled Receptor Oligomerisation. *Trends Pharmacol. Sci.* **39** 175-186.
[50] Chen Y, Wei LN, and Muller JD 2003 Probing protein oligomerization in living cells with fluorescence fluctuation spectroscopy. *Proc. Natl. Acad. Sci. U. S. A.* **100** 15492-15497.
[51] Stoneman MR, Biener G, Ward RJ, Pediani JD, Badu D, Eis A, Popa I, Milligan G, and Raicu V 2019 A general method to quantify ligand-driven oligomerization from fluorescence-based images. *Nat Methods* **16** 493-496.
[52] Stoneman MR, Biener G, and Raicu V 2020 Reply to: Spatial heterogeneity in molecular brightness. *Nat Methods* **17** 276-278.
[53] Sinclair MB, Haaland DM, Timlin JA, and Jones HDT 2006 Hyperspectral confocal microscope. *Applied Optics* **45** 6283-6291.

[54] Raicu V, Fung R, Melnichuck M, Chaturvedi A, and Gillman D. Combined spectrally-resolved multiphoton microscopy and transmission microscopy employing a high-sensitivity electron-multiplying CCD camera. in *Multiphoton Microscopy in the Biomedical Sciences VII*. 2007.
[55] Zhang ZY, Kenny SJ, Hauser M, Li W, and Xu K 2015 Ultrahigh-throughput single-molecule spectroscopy and spectrally resolved super-resolution microscopy. *Nat Methods* **12** 935-938.
[56] Biener G, Stoneman MR, Acbas G, Holz JD, Orlova M, Komarova L, Kuchin S, and Raicu V 2014 Development and Experimental Testing of an Optical Micro-Spectroscopic Technique Incorporating True Line-Scan Excitation. *Int. J. Mol. Sci.* **15** 261-276.
[57] Elliott AD, Gao L, Ustione A, Bedard N, Kester R, Piston DW, and Tkaczyk TS 2012 Real-time hyperspectral fluorescence imaging of pancreatic beta-cell dynamics with the image mapping spectrometer. *J. Cell Sci.* **125** 4833-4840.
[58] Lavagnino Z, Dwight J, Ustione A, Nguyen TU, Tkaczyk TS, and Piston DW 2016 Snapshot Hyperspectral Light-Sheet Imaging of Signal Transduction in Live Pancreatic Islets. *Biophys. J.* **111** 409-417.
[59] Neher R and Neher E 2004 Optimizing imaging parameters for the separation of multiple labels in a fluorescence image. *J. Microsc.* **213** 46-62.
[60] Thaler C, Koushik SV, Blank PS, and Vogel SS 2005 Quantitative multiphoton spectral imaging and its use for measuring resonance energy transfer. *Biophys. J.* **89** 2736-2749.
[61] Zimmermann T, Rietdorf J, Girod A, Georget V, and Pepperkok R 2002 Spectral imaging and linear un-mixing enables improved FRET efficiency with a novel GFP2-YFP FRET pair. *FEBS Lett.* **531** 245-249.
[62] Bacia K, Petrasek Z, and Schwille P 2012 Correcting for Spectral Cross-Talk in Dual-Color Fluorescence Cross-Correlation Spectroscopy. *Chemphyschem* **13** 1221-1231.
[63] Digman MA, Gratton E, Wiseman P, and Horwitz R 2009 Multicolor Fluctuation Spectroscopy in Cells: Obtaining the Stoichiometry of Molecular Complexes. *Biophys. J.* **96** 208a-208a.
[64] Chen Y, Tekmen M, Hillesheim L, Skinner J, Wu B, and Muller JD 2005 Dual-color photon-counting histogram. *Biophys. J.* **88** 2177-2192.
[65] Foust DJ, Ustione A, and Piston DW 2019 Spatial Cumulant Analysis to Study D2-Like Dopamine Receptor Dynamics on Plasma Membrane. *Biophys. J.* **116** 439a-439a.
[66] Unruh JR and Gratton E 2008 Analysis of molecular concentration and brightness from fluorescence fluctuation data with an electron multiplied CCD camera. *Biophys. J.* **95** 5385-98.